CrystEngComm

Accepted Manuscript

Journal Name

ARTICLE

Zinc ions to control the size of Yb/Er: $KMnF_3$ nanocrystals with single band emission

Received 00th January 20xx,
Accepted 00th January 20xx

DOI: 10.1039/x0xx00000x

www.rsc.org/

Lei Lei, Jiajia Zhou, Junjie Zhang, and Shiqing Xu*

Yb/Er co-doped $KMnF_3$ nanocrystals (NCs) exhibit strong single band emission centered at 660nm, which is beneficial for bio-imaging application. It is known that the bio-distribution, clearance rate, and elimination pathway of the intravenously injected NCs are strongly associated with the particle size. Here, we provide a novel method to modify the size of Yb/Er: $KMnF_3$ NCs by introducing Zn^{2+} in the initial solution. Through changing the concentration of Zn^{2+} (0 – 30 mol%), the size of Yb/Er: $KMnF_3$ NCs with cubic phase can be easily tuned from 8nm to 18nm. Interestedly, the Zn^{2+} did not incorporate into the lattice structure or adhere on the surface of the final NCs, it just helped the growth of Yb/Er: $KMnF_3$ NCs. Combined with the upconversion emission spectra results, we can provide a direct evidence for the size-dependent upconversion luminescence due to the final NCs with different sizes have same component, shape, crystal structure and crystallinity.

Introduction

Upconversion (UC) nanocrystals (NCs) have been widely investigated as a new class of luminescent labels and as alternatives to conventional labels, such as organic fluorophores and quantum dots, applied in biological imaging [1-21]. Yb/Er co-doped $NaYF_4$ NCs, which is regarded as the most efficient UC matrix due to its unique crystal structure, usually exhibit strong green emission (~550nm) and weak red emission (~660nm) [22-28]. However, it is believed that the near-infrared (NIR) spectral range (700-1100nm) and the red region (600-700nm) are referred to "optical window" of the biological tissues [29-30]. From this view of the point, the system of Yb/Er co-doped $NaYF_4$ NCs is limited in practical application due to its low penetration depth of green light and weak signal of red emission with low intensity.

Recently, the Mn^{2+}-contained materials, such as Mn/Yb/Er: $NaYF_4$ NCs [31], Yb/Er: $NaMnF_3$ NCs [32], and Yb/Er: $KMnF_3$ NCs [33], attracted much attention, because Mn^{2+} can receive energy from the $^2H_{9/2}$ and $^4S_{3/2}$ levels of Er^{3+} and then transfer to the $^4F_{9/2}$ level of Er^{3+} followed by strong red emission. For example, Liu's group reported that Yb/Er co-doped $KMnF_3$ NCs exhibit strong single band emission centered at 660nm, which is beneficial for bio-imaging application [33]. It is known that the bio-distribution, clearance rate, and elimination pathway of the intravenously injected NCs are strongly associated with the particle size [34]. Unfortunately, to the best of our knowledge, there is no report about controlling the size of Yb/Er: $KMnF_3$ NCs until now.

So far, several methods are used to tune the size of fluorides NCs, such as ion-doping, changing the reaction temperature or time, varying the concentration of precursor chemicals or the ratio of solvent [35-42]. However, these traditional methods may change the component, crystallinity or morphology of the final products. Here, we provide a novel method to modify the size of Yb/Er: $KMnF_3$ NCs by introducing Zn^{2+} in the reaction system. Through tuning the concentration of Zn^{2+} ions (10 – 30 mol%), different sizes of Yb/Er: $KMnF_3$ NCs with cubic phase can be obtained. Interestedly, the Zn^{2+} did not incorporate into the lattice structure or adhere on the surface of the final NCs, it just helped the growth of Yb/Er: $KMnF_3$ NCs. In addition, all the samples were prepared under the same experiment condition except the different ratio of Mn : Zn in the precursor solution. In this case, the final NCs with different sizes have same component, shape, crystal structure and crystallinity,

College of Materials Science and Engineering, China Jiliang University, Hangzhou 310018, China. E-mail: shiqingxu75@163.com; Fax: +86 57186875607; Tel: +86 57186875607
Electronic Supplementary Information (ESI) available. See DOI: 10.1039/x0xx00000x

which can provide a direct evidence for the size-dependent upconversion luminescence.

Experimental

Materials. All chemicals were of analytical grade and were used as received without further purification. Deionized water was used throughout. $LnCl_3 \cdot 6H_2O$ (Ln=Yb, Er), $Mn(CH_3COO)_2 \cdot 4H_2O$, $C_4H_6O_4Zn \cdot 2H_2O$, KF, 1-octadecene (ODE), oleic acid (OA), Oleylamine (OM), cyclohexane and ethanol were all supplied by Sinopharm Chemical Reagent Company.

Synthesis of Ln-acetylacetonate (Ln= Yb, Er) (named Yb(acac)$_3$, Er(acac)$_3$) precursor. Take Yb(acac)$_3$ as an example, 2mL HNO_3 were added to 30 mL aqueous solution containing 10 mmol $YbCl_3 \cdot 6H_2O$ to form solution A, 8 mL acetylacetonate, 6mL $NH_3 \cdot H_2O$ and 20mL H_2O were mixed together to form solution B, and mixed with solution A. Then adjusting PH of the above mixed solution at 6~7 through adding $NH_3 \cdot H_2O$ or HNO_3. The resulted solution maintained at room temperature for 2h, then washed with water for three times and finally dried at 60 ^oC to obtain Yb(acac)$_3$ powder. Er(acac)$_3$ powder was prepared by a similar method, except that $YbCl_3 \cdot 6H_2O$ was substituted by $ErCl_3 \cdot 6H_2O$.

Synthesis of Yb/Er: $KMnF_3$ NCs with different Zn^{2+} concentration in the initial solution. The Yb/Er: $KMnF_3$ NCs with different Zn^{2+} concentration in the initial solution were prepared in three steps according to a modified literature procedure [43]. $Mn(CH_3COO)_2 \cdot 4H_2O$ (0.8mmol × (0.8-y)), $C_4H_6O_4Zn \cdot 2H_2O$ (0.8mmol × y, y= 0, 0.1, 0.2, 0.3, 0.4), Yb(acac)$_3$ (0.8mmol × 0.18), Er(acac)$_3$ (0.8mmol × 0.02) were added to a 50 mL flask containing 4mL OA and 4mL OM. The mixture was heated at 150 ^oC for 30 min to remove water from the solution. Then 12mL ODE was quickly added to the flask and the mixture was heated at 150 ^oC for another 30 min to form a clear solution, and then cooled down to room temperature. Afterwards, 6ml methanol solution containing KF 2 mmol was added into the above solution and stirred at 70^oC for 30 min. After the methanol was evaporated, the solution was heated at 80 ^oC for 5 min, and further heated at 280 ^oC under N_2 for 90 min and then cooled down to room temperature. The products were precipitated by addition of ethanol, collected by centrifugation, washed with cyclohexane and ethanol for three times, and finally dried at 60 ^oC.

Characterizations.

XRD analysis was carried out with a powder diffractometer (DMAX2500 RIGAKU) using Cu-K$_a$ radiation (λ=0.154 nm). The size, shape and uniformity of the products were studied using a transmission electron microscope (TEM, JEM-2010) equipped with an energy dispersive X-ray spectroscope (EDS). TEM specimens were prepared by directly drying a drop of a dilute cyclohexane dispersion solution of the products on the surface of a carbon coated copper grid. UC emission spectra were recorded on an Edinburgh Instruments FLS920 spectrofluorimeter equipped with an adjustable laser diode (976 nm) as the excitation sources. To enable comparison of the UC emission intensities among different samples, the emission spectra were measured with the same instrumental parameters (for example: same mass of samples, same excitation wavelength and power, same excitation and emission slits, and so on). All the measurements were carried out at room temperature.

Results and discussion

X-ray diffraction (XRD) patterns of the final products with different Zn^{2+} content (0, 10, 20 to 30 mol%) in the initial solution are shown in Fig.1. All the XRD peaks of those products match well with the cubic $KMnF_3$ phase (JCPDS 17-0116). Further increasing Zn^{2+} content to 40% or 50%, along with the cubic $KMnF_3$ phase, a small part of impurity ZnF_2 phase emerged (Fig. S1). In cubic $KMnF_3$ crystal structure, Mn^{2+} ions locate at the body-center, F^- ions lie at the face-center, and K^+ ions occupy the nodes of the cubic lattice (Fig. 1b). The Ln^{3+} (Ln= Yb, Er) ions will incorporate into the $KMnF_3$ crystal lattice by substituting Mn^{2+} after adding Ln^{3+} into the reaction system. It should be noted that charge balance in $KMnF_3$ is disturbed after Ln^{3+} replacing Mn^{2+}, so K^+ or Mn^{2+} vacancies formed to maintain charge balance [32].

Transmission electron microscope (TEM) observations indicate that the size of the final products with cubic shape increases gradually with increasing Zn^{2+} concentration in the initial reaction system (Fig. 2). The mean sizes of those NCs are measured to be about 8nm, 12nm, 14nm and 18nm, respectively, as exhibited in

Fig. 2f. The selected area electron diffraction (SAED) pattern suggests that the corresponding NCs are of cubic structure (inserted in Fig. 2b). The lattice fringes are clearly observed, and the d-spacing is measured to be about 0.42nm, corresponding to the (100) plane of cubic $KMnF_3$ phase (Fig. 2e).

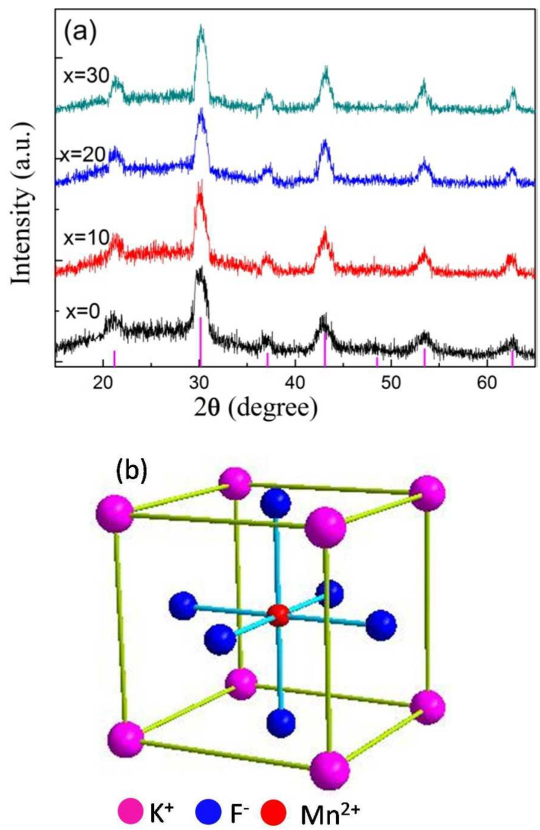

Fig. 1 (a) XRD patterns of Yb/Er: $KMnF_3$ NCs prepared under different Zn^{2+} concentration x% (x=0, 10, 20, 30); (b) the crystal structure of cubic $KMnF_3$.

To explore the mechanism of Zn^{2+} ions in the reaction system induce size variation of Yb/Er: $KMnF_3$, it is necessary to clarify the location of those Zn^{2+} ions. As shown in Fig. 1a, there is no detectable position shifting of XRD peaks with different Zn^{2+} content although the radius of Zn^{2+} (0.1065 nm) is smaller than that of Mn^{2+} (0.1278 nm) [44]. In addition, the energy dispersive X-ray spectroscopy (EDS) results indicate that there is no signal of Zn element in the products prepared with and without Zn^{2+} (Fig. S2). The XRD and EDS results confirm the absence of Zn^{2+} ions in Yb/Er: $KMnF_3$ NCs with different sizes, including the crystal lattice and surface of the NCs.

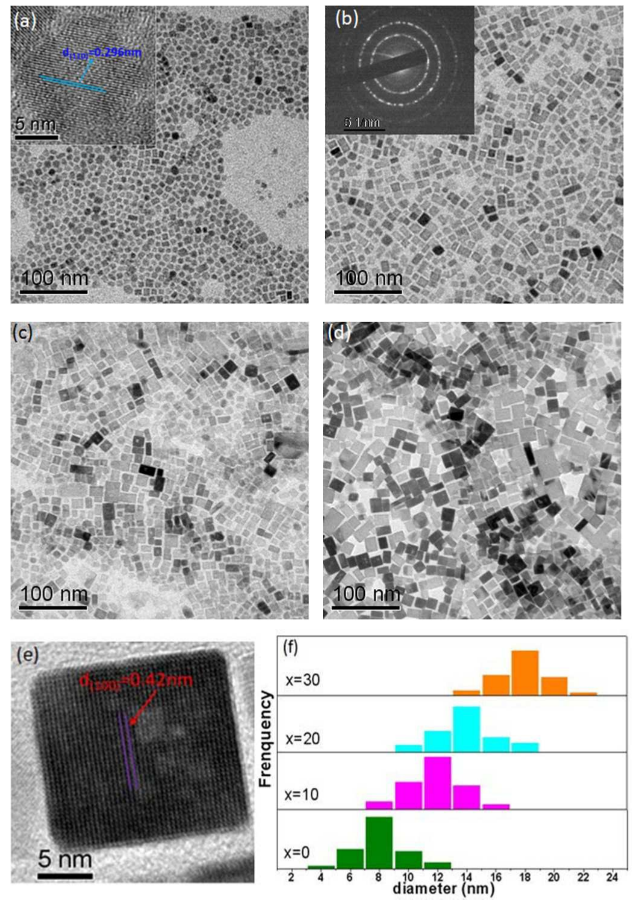

Fig. 2 TEM images of Yb/Er: $KMnF_3$ NCs prepared under different Zn^{2+} concentration x% : (a) x=0, (b) x=10, (c) x=20, (d) x=30; Insert of (a) shows HRTEM image of an individual NC, inset of (b) shows its corresponding SAED pattern; (e) HRTEM image of an individual NC in (d); (f) histograms of particle size distribution of Yb/Er: $KMnF_3$ NCs with different Zn^{2+} concentration in the initial reaction system.

To further determine the effect of Zn^{2+} on Yb/Er: $KMnF_3$ NCs growth, two comparable samples, including Yb/Er: $KMnF_3$ NCs with Zn^{2+} : Mn^{2+} ratio of 30: 70 (increase Mn^{2+} concentration to 70% and Zn^{2+} concentration remain at 30%, named A) and Yb/Er: $KMnF_3$ NCs with Zn^{2+} : Mn^{2+} ratio of 0: 50 (remove Zn^{2+} precursor and Mn^{2+} concentration remain at 50%, named B), were prepared and characterized. As shown in Fig. S3a, the sample A is belonged to pure $KMnF_3$ phase. Its mean size is larger than the sample in Fig. 2a (Zn^{2+} : Mn^{2+} ratio at 0: 70), but smaller than the sample in Fig. 2d

(Zn^{2+} : Mn^{2+} ratio at 30: 50). The sample B contains two mixed phases, including KYb_3F_{10} and $KMnF_3$ (Fig. S3b), and the mean particle size of those $KMnF_3$ NCs is also decreased in comparison with the sample in Fig. 2d (Fig. 3b). In one word, increasing Mn^{2+} ions or decreasing Zn^{2+} ions concentration, which mean that Zn^{2+} content around a single Mn^{2+} ion in a certain volume decrease, results in the mean size of the final products reduce. These results suggest that Zn^{2+} can promote the growth of $KMnF_3$ NCs. With prolonging the reaction time to 5h, the ZnF_2 phase emerged, except $KMnF_3$ phase (Fig. S4). In addition, we found that the mean particle size of Yb/Er: $KMnF_3$ NCs prepared without Zn^{2+} in the initial solution increased after F^- content increased from 2.0mmol to 2.4mmol (Fig. S5), which suggests that F^- can also promote the growth of $KMnF_3$ NCs. It should be noted that the morphology goes worse with increasing F^- concentration.

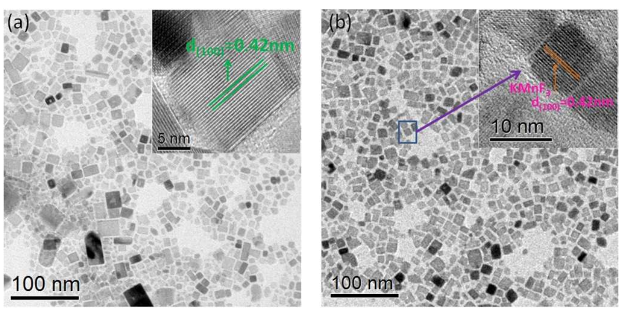

Fig. 3 TEM images of Yb/Er: $KMnF_3$ NCs with an Zn^{2+} : Mn^{2+} ratio of 30: 70 (a) and Yb/Er: $KMnF_3$ NCs with an Zn^{2+} : Mn^{2+} ratio of 0: 50 (b), inserts shows the corresponding HRTEM images.

According to the above results, a possible mechanism about Zn^{2+} promotes the growth of Yb/Er: $KMnF_3$ NCs in our system is proposed, as schematically illustrated in Fig. 4. At first, Mn^{2+} and Yb^{3+}/Er^{3+} combined with oleic acid molecules to form metal-oleat complexes, then react with K^+ and F^- to form Yb/Er: $KMnF_3$ nuclei. Along with the reaction, these nuclei grow up and the monodispersed Yb/Er: $KMnF_3$ NCs formed with OA as surfactant. In the case of adding Zn^{2+} ions into the system, the reaction process is different. Mn^{2+} is a harder Lewis acid compared to Zn^{2+}, so the Zn^{2+} is significantly more reactive than Mn^{2+} if they both have the same carboxylate ligand [45]. In this case, after the zinc-oleat molecules are linked to the surface of the Yb/Er: $KMnF_3$ nuclei due to Brownian motion of those molecules, the diffusion rate of F^- ions from the solution to the nuclei is faster than that of without Zn^{2+} situation. Afterwards, the K^+ and Mn^{2+} cations in the solution react with F^- anions on the nuclei surface and results in the growth of the nuclei. With increasing Zn^+ concentration, the nuclei attract more F^-, K^+ and Mn^{2+} ions, and then grow bigger than before. After the depletion of Mn^{2+} in the solution, the growth of Yb/Er: $KMnF_3$ NCs is terminated. The Zn^{2+} ions on the surface of $KMnF_3$ NCs and in the solution can be washed away by cyclohexane and ethanol, which can be verified by the EDS results. With prolonging the reaction time, the Zn^{2+} combined with the superfluous F^- to form ZnF_2 phase. The ZnF_2 phase can be avoided through controlling the experiment condition, which indicates that $KMnF_3$ phase is more stable than ZnF_2 phase in our reaction system. Hence, even a part of F^- combine with Zn^{2+} to form ZnF_2 in the reaction process, it would dissolve quickly, and then those escaped F^- still can promote the growth of $KMnF_3$ nuclei.

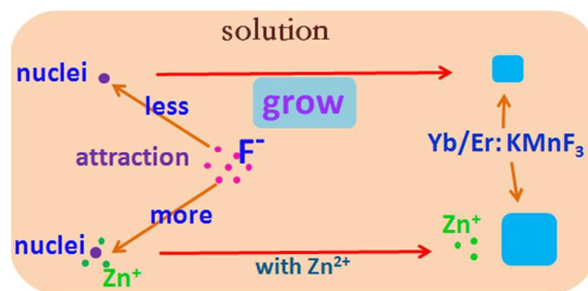

Fig. 4 Schematic illustration of the mechanism about Zn^{2+} promotes the growth of Yb/Er: $KMnF_3$ NCs

The UC spectra of Yb/Er: $KMnF_3$ NCs with different sizes are shown in Fig. 5a. Under 976nm laser excitation, all the samples exhibit single-band emission centered at 655nm, corresponding to $^4F_{9/2}\rightarrow{}^4I_{15/2}$ transition. The UC emission intensity enhanced gradually with the size increased (Fig. 5b). It has been reported smaller particles have weaker UC emissions due to the surface quenching effect. Actually, in most of the size-dependent UC emission cases, the varying parameter is not only containing size, but some others. For example, by the traditional methods of tuning the size of fluorides NCs, changing the reaction temperature or time will change the crystallinity of NCs, varying the concentration of precursor chemicals or the ratio of solvents will vary the morphology of NCs, doping different ions will alter the composition of NCs. However, in our experiment, all the final NCs with different sizes are prepared under the same reaction condition except the diverse ratio of Mn^{2+} : Zn^{2+} and the Zn^{2+} ions did not incorporate into the lattice structure or adhere on the surface of the final NCs. Hence, these products have same component, morphology, crystal structure and crystallinity, which can provide a direct evidence for the size-dependent upconversion luminescence. In our case, the emission intensity enhanced about 7, 11, and 24 times with the mean size of the Yb/Er: $KMnF_3$ NCs increased from 8nm to 12nm, 14nm, and 18nm, respectively. For UC materials, a long lifetime usually means a highly-efficient UC luminescence [46-49]. As revealed in Figure S8, the trend of lifetime variation is consistent with that of UC intensity variation. This can be explained by the greater multi-phonon relaxation probabilities of Er^{3+} in smaller NCs having a high surface-to-volume ratio, so that a larger proportion of Er^{3+} ions are located on the surfaces and under the influence of high energy vibration groups such as stabilizing ligands, solvent molecules and surface defects.

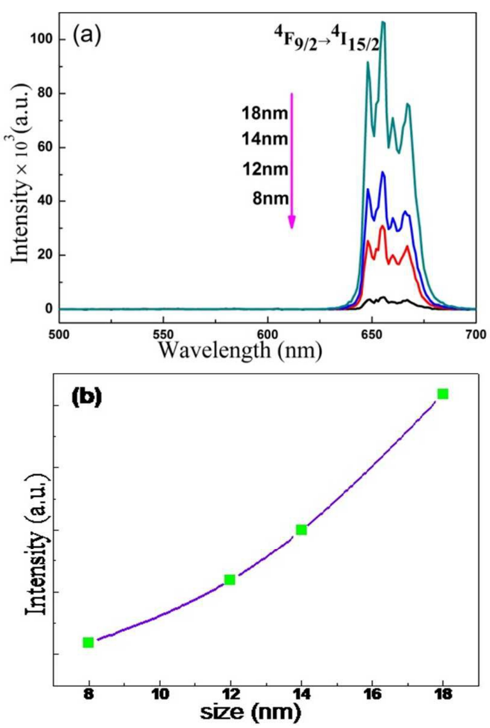

Fig. 5 (a) upconversion spectra of Yb/Er: $KMnF_3$ NCs with different sizes (8nm, 12nm, 14nm, 18nm), (b) total emission intensities versus size.

For a UC luminescence process, the UC emission intensity (I_{UC}) is proportional to the n-power of the excitation (I_{IR}) power:

$$I_{UC} \propto I_{IR}^{\ n}$$

where n is the absorbed photon numbers per visible photon emitted, and its value can be obtained from the slope of the fitted line of the plot of log(I_{UC}) versus log(I_{IR}). As shown in Fig. S6, n value of the red emission for Yb/Er: $KMnF_3$ NCs with 8nm and 14nm are 1.80 and 1.84, respectively, indicateing the red emission proceeds via a two photon process and the UC mechanism is not affected when the size changed from 8nm to 14nm. The possible UC emission mechanism is shown in Fig. S7.

For practical applications, thermal stability of upconversion nanocrystals is a crucial parameter, and the working temperature of most luminescent devices is usually above room temperature (RT). Hence, it is important to investigate the temperature-dependent UC emissioin intensity of Yb/Er: $KMnF_3$ NCs. The integrated red emission intensity of Yb/Er: $KMnF_3$ NCs with 18nm at various temperatures are exhibited in Fig. 6. With increasing temperature from 298K to 473K, the UC emission intensity decreases gradually, while its intensity increases gradually with the temperature cooling to RT, and the efficiency is as high as before. These results indicate that the Yb/Er: $KMnF_3$ NCs can be applied in a certain high temperature field.

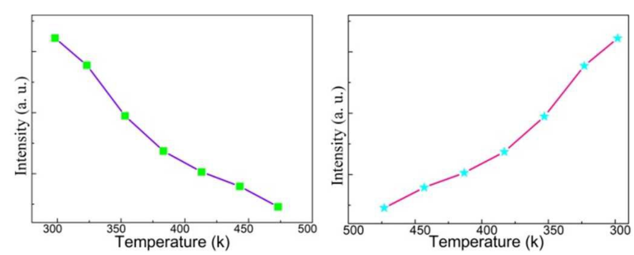

Fig. 6 The integrated red emission intensity of Yb/Er: $KMnF_3$ NCs with 18nm at various temperatures during heating and cooling, respectively.

Conclusions

In summary, this study offers a novel method to modify the size of Yb/Er: $KMnF_3$ NCs through introducing Zn^{2+} in the initial solution. The size of Yb/Er: $KMnF_3$ NCs with cubic phase can be easily tuned from 8nm to 18nm by changing the concentration of Zn^{2+} ions (0 – 30 mol%). Interestedly, the Zn^{2+} did not incorporate into the lattice structure or adhere on the surface of the final NCs, and all the samples were prepared under the same reaction condition except the different ratio of Mn : Zn in the precursor solution, so the final NCs with different sizes have same component, shape, crystal structure and crystallinity. Hence, these results can provide a direct evidence for the size-dependent upconversion luminescence.

Acknowledgements

This work was supported by International Science & Technology Cooperation Program of China (No.2013DFE63070), and the national Natural Science Foundation of China (No. 51472225, 11404311, 51372235 and 51272242), Zhejiang Provincial Natural Science Foundation of China (No. LY14E020007 and LR14E020003).

References

1 F. Wang, Y. Han, C. S. Lim, Y. H. Lu, J. Wang, J. Xu, H. Y. Chen, C Zhang, M. H. Hong, and X. G. Liu, Nature 2010, **463**,1061.

2 J. B. Zhao, D. Y. Jin, E. P. Schartner, Y. Q. Lu, Y. J. Liu, A. V. Zvyagin, L. X. Zhang, J. M. Dawes, P. Xi, J. A. Piper, E. M. Goldys, and T. M. Monro, Nature Nanotechnology, 2013, 8, 729.

3 F. Auzel, Chem.Rev. 2004, **104**, 139.

4 Daqin Chen, Ping Huang, Dalton Trans., 2014, **43**, 11299.

5 M. Haase, and Helmut Schäfer, Angew. Chem. Int. Ed. 2011, **50**, 5808.

6 R. R. Deng, X. J. Xie, M. Vendrell, Y. T. Chang, and X. G. Liu, J. Am. Chem. Soc. 2011, **133**, 20168.

7 G. Y. Chen, T. Y. Ohulchanskyy, A. Kachynski, H. Ågren, and P. N. Prasad, ACS Nano, 2011, **5**, 4981.

8 D. Q. Chen, Z. Y. Wan, Y. Zhou, W. D. Xiang, J. S. Zhong, M. Y. Ding, H. Yu, Z. G. Ji, J. Mater. Chem. C, 2015, **3**, 3141.

9 Y. F. Wang, L. D. Sun, J. W. Xiao, W. Feng, J. C. Zhou, J. Shen, C. H. Yan, Chem. Eur. J. 2012, **18**, 5558.

10 D. C. Yu, X. Y. Huang, S. Ye, M. Y. Peng, Q. Y. Zhang, L. Wondraczek, Appl. Phys. Lett., 2011, **99**, 161904

11 T. Y. Cao, Y. Yang, Y. Gao, J. Zhou, Z. Q. Li, F. Y. Li, Biomaterials 2011, **32**, 2959.

12 G. F. Wang, Q. Peng, Y. D. Li, J. Am. Chem. Soc. 2009, **131**, 14200.

13 Y. P. Du, Y. W. Zhang, Z. G. Yan, L. D. Sun, C. H. Yan, J. Am. Chem. Soc. 2009, **131**, 16364.

14 Y. P. Du, Y. W. Zhang, L. D. Sun, C. H. Yan, J. Am. Chem. Soc. 2009, **131**, 3162.

15 Y. L. Dai, H. H. Xiao, J. H. Liu, Q. H. Yuan, P. A. Ma, D. M. Yang, C. X. Li, Z. Y. Cheng, Z. Y. Hou, P. P. Yang, J. Lin, J. Am. Chem. Soc., 2013, **135**, 18920.

16 D. Q. Chen, Y. Chen, H. W. Lu, Z. G. Ji, Inorg. Chem., 2014, **53**, 8638.

17 Q. Liu, Y. Sun, T. S. Yang,W. Feng, C. G. Li,Y. F. Li. J. Am. Chem. Soc. 2011, **133**, 17122.

18 N. Niu,P. P. Yang, F. He,X. Zhang, S. L. Gai,C. X. Li, J. Lin, J. Mater. Chem. 2012**, 22**, 10889.

19 Y. S. Liu, D. T. Tu, H. M. Zhu, R. F. Li, W. Q. Luo, X. Y. Chen, Adv. Mater. 2010, **22**, 3266.

20 P. Huang, W. Zheng, S. Y. Zhou, D. T. Tu, Z. Chen, H. M. Zhu, R. F. Li, E. Ma, M. D. Huang, X. Y. Chen, Angew. Chem. Int. Ed. 2014, **53**, 1252.

21 Z. Song, Y. G. Anissimov, J. B. Zhao, A. V. Nechaev, A. Nadort, D. Y. Jin, T. W. Prow, M. S. Roberts, A. V. Zvyagin, J. Biomed. Opt. 2013, **18**, 061215

22 J. C. Boyer, F. Vetrone, L. A. Cuccia, J. A. C apobianco, J. Am. Chem. Soc. 2006, **128**, 7444.

23 F. Wang, X. G. Liu, J. Am. Chem. Soc. 2008, **130**, 5642

24 C. H. Liu, H. Wang, X. R. Zhang, D. P. Chen, J. Mater. Chem. 2009, **19**, 489.

25 F. Shi, J. S. Wang, X. S. Zhai, D. Zhao, W. P. Qin, CrystEngComm, 2011, **13**, 3782.

26 D. T. Tu, Y. S. Liu, H. M. Zhu, R. F. Li, L. Q. Liu, and X. Y.Chen, Angew. Chem. 2012, **124**, 1.

27 K. W. Krämer, D. Biner, G. Frei, H. U. Güdel, M. P. Hehlen, S. R. Lüthi, Chem. Mater. 2004, **16**, 1244.

28 P. Ptacek, H. Schäfer, K. Kömpe, M. Haase, Adv. Funct. Mater. 2007, **17**, 3843.

29 R. G. Aswathy, Y.Yoshida, T. Maekawa, D. S. Kumar, Anal. Bioanal. Chem. 2010, **397**, 1417.

30 Y. T. Zhong, G. Tian, Z. J. Gu, Y. J. Yang, L. Gu, Y. L. Zhao, Y. Ma, and J. N. Yao, Adv. Mater. 2014, **18**, 2831.

31 G. Tian, Z. J. Gu, L. J. Zhou, W. Y. Yin, X. X. Liu, L. Yan, S. Jin, W. L. Ren, G. M. Xing, S. J.Li, and Y. L. Zhao, Adv. Mater. 2012, **24**, 1226.

32 Y. Zhang,a J. D. Lin, V. Vijayaragavan, K. K. Bhakoob, and T. T. Y. Tan, Chem. Commun., 2012, **48**, 10322.

33 J. Wang, F. Wang, C. Wang, Z. Liu, and X. G. Liu, Angew. Chem. Int. Ed. 2011, **50**, 1.

34 Y. Hou, R. R. Qiao, F. Fang, X. X. Wang, C. Y. Dong, K. Liu, C. Y. Liu, Z. F. Liu, H. Lei, F. Wang, M. Y. Gao, ACS Nano, 2013, **7**, 330.

35 D. Q. Chen, Y. L. Yu, F. Huang, P. Huang, A. P. Yang, and Y. S. Wang, J. Am. Chem. Soc. 2010, **132**, 9976.

36 L. Lei, D. Q. Chen, P. Huang, J. Xu, R. Zhang, and Y. S. Wang, Nanoscale, 2013,**5**, 11298.

37 L. Y. Wang, and Y. D. Li, Chem. Mater. 2007, **19**, 727.

38 J. L. Zhuang, L. F. Liang, H. H. Y. Sung, X. F. Yang, M. M. Wu, I. D. Williams, S. H. Feng, and Q. Su, Inorg. Chem. 2007, **46**, 5404.

39 S. J. Zeng, G. Z. Ren, C. F. Xu, and Q. B. Yang, CrystEngComm, 2011, **13**, 1384.

40 H. X. Mai, Y. W. Zhang, R. Si, Z. G. Yan, L. D. Sun, L. P. You, and C. H. Yan, J. Am. Chem. Soc. 2006, **128**, 6426.

41 H. X. Mai, Y. W. Zhang, L. D. Sun, and C. H. Yan, J. Phys. Chem. C, 2007, **111**, 13730.

42 D. M. Yang, X. J. Kang, M. M. Shang, G. G. Li, C. peng, C. X. Li, and J. Lin, Nanoscale, 2011, **3**, 2589.

43 Z. Q. Li, and Y. Zhang, Nanotechnology, 2008, **19**, 345606.

44 U. Hohm, and A. J. Thakkar, J. Phys. Chem. A, 2012, **116**, 697.

45 N. Pradhan, D. Goorskey, J. Thessing, and X. G. Peng, J. Am. Chem. Soc. 2005, **127**, 17586.

46 D. Y. Jin, and J. A. Piper, Anal. Chem. 2011, **83**, 2294.

47 F. Shi, J. S. Wang, X. S. Zhai, D. Zhao, and W. P. Qin, CrystEngComm, **2011,** *13*, 3782.

48 J. Lu, L. T. Paulsen, and D. Y. Jin, Anal. Chem. 2013, **85**, 8240.

49 J. B. Zhao, Z. D. Lu, Y. D. Yin, C. McRae, J. A. Piper, J. M. Dawes, D. Y. Jin, and E. M. Goldys. Nanoscale, 2013, **5**, 944.

Graphic Abstract

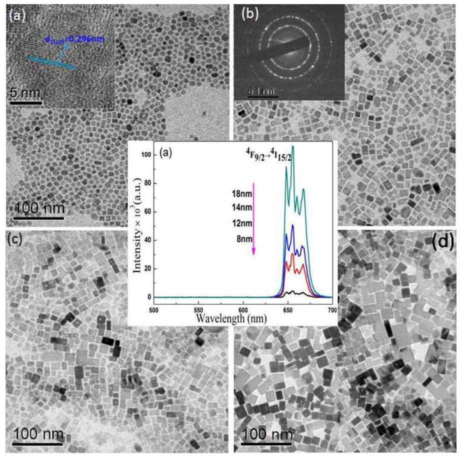

A novel method to modify the size of Yb/Er: $KMnF_3$ NCs by introducing Zn^{2+} in the initial solution, and the results can provide direct evidence for the size-dependent upconversion luminescence.